Manuscript Draft

Manuscript Number:

Title: First-order phase transition and large magnetocaloric effect in particulate equiatomic FeRh alloy

Article Type: Full Length Article

Keywords: Magnetocaloric effect; Micrometers; Solid-phase reactions; X-ray diffraction; Electron microscopy; Iron-rhodium

Corresponding Author: Professor Hao Fu,

Corresponding Author's Institution: University of Electronic Science and Technology of China

First Author: Yutao Cao, Master

Order of Authors: Yutao Cao, Master; Yue Yuan, bachelor; Yafen Shang, Doctor; Vladimir I Zverev; Radel R Gimaev; Radhika Barua; Ravi L Hadimani; Lan Mei; Gang Guo; Hao Fu

Abstract: Micro-sized particles of FexRh100-x (x = 50, 48, 45, 40, and 35) binary alloys were synthesized by a solid phase reduction method and their structural and magnetic properties have been characterized. From X-ray diffraction results, the Fe50Rh50 alloy is in a single chemically ordered α' phase while the face-centered cubic disordered γ phase arises and increases with Rh content when x is smaller than 50. The magnetization behavior of the alloys demonstrates the α' phase consists of ferromagnetic and antiferromagnetic components due to the nonuniformity of elements in the particulate alloys. The maximal magnetic entropy changes and relative refrigeration capacity of the Fe50Rh50 particles reaches 9.7 J/kg K and 230 J/kg, respectively, with a 0-3 T magnetic field change. Large magnetocaloric effect and low biologically toxicity make the Fe50Rh50 alloy promising for biomedical applications.

Research Data Related to this Submission

There are no linked research data sets for this submission. The following reason is given:

Data will be made available on request

Cover Letter

Dear Editor:

We submit our manuscript titled "First-order phase transition and large

magnetocaloric effect in particulate equiatomic FeRh alloy" to your JOURNAL OF

ALLOYS AND COMPOUNDS for consideration and publication.

We synthesized micro-sized particles of Fe_xRh_{100-x} (x = 50, 48, 45, 40, and 35)

binary alloys by a solid phase reduction method and characterized their structure and

magnetic properties. The chemically ordered bcc α' single-phase was successfully

obtained in the Fe₅₀Rh₅₀ particles. Unlike the Fe₅₀Rh₅₀ nanoparticle, micro-sized

Fe₅₀Rh₅₀ particles exhibit evident first-order transition near 350 K, large magnetic

entropy change, 9.7 J/kgK, and relative cooling power, 211 J/kg, for $\Delta H = 3$ T. New

features, such as large thermal hysteresis, great residual magnetization after the

FM-AFM transition, which are different from both bulk and nano-sized Fe₅₀Rh₅₀

counterparts, are also observed and the reasons are discussed. In addition, in vitro

biological toxicity test of FeRh particles supports the possible feasibility of Fe-Rh

particles in biomedical applications.

By submitting this paper to your journal, we confirm that no part of this paper or

its entirety has been published or accepted for publication anywhere else.

All authors, Yutao Cao, Yue Yuan, Yafen Shang, Vladimir I. Zverev, Radel R.

Gimaev, R. Barua, R. L. Hadimani, Lan Mei, Gang Guo, Hao Fu, have approved the

submission of our manuscript to your journal.

Thank you very much for your attention.

Sincerely,

Hao Fu

Email: fuhao@uestc.edu.cn

Prime Novelty Statement

In this work, we propose an approach to synthesize Fe-Rh particles with such magnetothermal and dimensional characteristics, study their structure as well as magnetic properties and explore the effects of elemental composition on their magnetocaloric response. Through this method, relatively pure and advantageous phase composition for Fe-Rh particles is realized. The particle samples show appreciable MCE with a ΔSmag maximum of about 9.7 J/Kg·K and an RCP of almost 230 J/kg under a magnetic field change of 0 to 3 T in an appropriate temperature interval as intended. The biological toxicity of Fe-Rh samples is also investigated for approving their potential use in biomedical applications.

First-order phase transition and large magnetocaloric effect in particulate equiatomic FeRh alloy

Yutao Cao¹, Yue Yuan², Yafen Shang¹, Vladimir I. Zverev³, Radel R. Gimaev⁴,

R. Barua⁵, R. L. Hadimani⁵, Lan Mei⁶, Gang Guo⁶, Hao Fu^{1*}

Author to whom correspondence should be addressed. Electronic mail: fuhao@uestc.edu.cn

Abstract

Micro-sized particles of Fe_xRh_{100-x} (x = 50, 48, 45, 40, and 35) binary alloys were synthesized by a solid phase reduction method and their structural and magnetic properties have been characterized. From X-ray diffraction results, the $Fe_{50}Rh_{50}$ alloy is in a single chemically ordered α' phase while the face-centered cubic disordered γ phase arises and increases with Rh content when x is smaller than 50. The magnetization behavior of the alloys demonstrates the α' phase consists of ferromagnetic and antiferromagnetic components due to the nonuniformity of elements in the particulate alloys. The maximal magnetic entropy changes and relative refrigeration capacity of the $Fe_{50}Rh_{50}$ particles reaches 9.7 J/kg K and 230 J/kg, respectively, with a 0-3 T magnetic field change. Large magnetocaloric effect and low biologically toxicity make the $Fe_{50}Rh_{50}$ alloy promising for biomedical applications.

Keywords: Magnetocaloric effect; Micrometers; Solid-phase reactions; X-ray diffraction; Electron microscopy; Iron-rhodium

Introduction

FeRh equiatomic alloy aroused wide interest for having the largest magnetocaloric effect (MCE) in term of the adiabatic temperature change $(\Delta T_{\rm ad} = 12.9~{\rm K~with}~\Delta H_{\rm app} = 2~{\rm T})~{\rm among~the~known~magnetocaloric~materials~which}$

¹ School of Physics, University of Electronic Science and Technology of China, Chengdu, 610054, People's Republic of China

² Glasgow College, University of Electronic Science and Technology of China, Chengdu, 611731, People's Republic of China

³ Faculty of Physics, M.V. Lomonosov Moscow State University, 119991 Moscow, Russia

⁴ National Research Center "Kurchatov Institute", Moscow 123182, Russia

⁵ Department of Mechanical and Nuclear Engineering, Virginia Commonwealth University, Richmond VA 23284, USA

⁶ State Key Laboratory of Biotherapy and Cancer Center, West China Hospital, Sichuan University, Chengdu, 610041, People's Republic of China

undergo the first order phase transition (FOPT). The CsCl-type (B2) crystalline structure of bulk near-equiatomic Fe-Rh alloys and their first-order metamagnetic phase transitions with large magnetic entropy changes up to 16 J/kg·K ($\Delta H_{app} = 2$ T) in the range of 320-390 K,² depending on the Rh content, drew this promising material system additional attention. Compared with extensively studied bulk and film Fe-Rh materials, researches on particulate Fe-Rh alloy are limited. The prior reports mainly focus on Fe-Rh nanoparticles, in which the Fe-Rh particles did not exhibit any MCE as bulk Fe-Rh alloys. For example, in the work of Barua et al., ^{3,4} FeRh nanoprecipitates (~10 nm) fabricated by thermal annealing rapidly solidified (FeRh)₅Cu₉₅ alloy are in L1₀-type (CuAu_{1-v}Pd_v) structure, undergoing an antiferromagnetic (AFM) to ferromagnetic (FM) transition near 130 K, which is far lower than that of the bulk Fe-Rh alloy. As for the studies of Ko et al., Fe_xRh_{100-x} (x =35-80) nanoparticles, whose grain size is 3-5 nm in average for as-deposited state, synthesized via solution phase chemical method possess α' phase accompanied by γ phase, where the AFM to FM first order transition is observed around 470 K for x =39.⁵⁻⁷ Coexistence of α' phase with γ phase and obvious AFM to FM transition around 350 K were also reported by Jia et al. in Fe₅₁Rh₄₉ nanoparticles (4-20 nm) synthesized by polyol co-reduction. Nevertheless, except Fe₃₉Rh₆₁ which is inconclusive due to the normalized ordinate of temperature dependent magnetization curve, other Fe-Rh nanoparticles only exhibit very limited magnetizations as low as 2×10^{-3} emu/g with applied field $\mu_0H=100$ Oe even in FM regions. These researches seem to imply the phase components and magnetic properties of Fe-Rh particles are

sensitive to the microstructural scale and fabrication procedure and nanoparticles are not ideal routes for distinct first-order transition feature or large MCE. The studies of the fabrication procedure influence, namely heat treatment, of bulk FeRh alloys prove this assumption for micro- and nanosized samples.¹⁰

Low frequency magnetic field penetrates biological tissues without attenuation and side effects, hence MCE is highly expected to applied in biomedical applications, for example, to realize local cooling or heating in a changing magnetic field for targeted drug delivery and magnetic hyperthermia. In this area, Fe-Rh alloys have great potential indicated by their MCE, transition temperatures in the vicinity of body temperature which also can be adjusted by doping Pd or Pt. In Ref.12, it has been suggested to use Fe-Rh alloys for magnetocaloric hyperthermia instead of traditional magnetic hyperthermia. Simultaneously, with heat impact the alloys being embedded in a polymeric matrix put on an implant surface would provide targeted drug delivery. Is

To serve such applications, the particles or films should be large enough in dimensions to guarantee sufficient refrigerating capacity. Nevertheless, the deposition method adopted in existing papers cannot produce thick Fe-Rh films on the order of micrometer or millimeter. It is well known that addictive manufacturing, such as 3D printing and low temperature spray, can produce thick coatings by utilizing powders as the raw materials. Thus, more work on particulate Fe-Rh alloys is desired.

In this context, we propose an approach to synthesize Fe-Rh particles with such magnetothermal and dimensional characteristics, study their structure as well as magnetic properties and explore the effects of elemental composition on their magnetocaloric response. Through this method, relatively pure and advantageous phase composition for Fe-Rh particles is realized. The particle samples show appreciable MCE in an appropriate temperature interval as intended. The biological toxicity of Fe-Rh samples is also investigated for approving their potential use in biomedical applications. Mouse fibroblast 3T3 cells were used. The cell viability was tested after 24 h when the cell was incubated with the extraction from FeRh prepared by PBS.

Experimental details

The FeRh equiatomic powder sample was synthesized by a high temperature solid state reaction from equimolar FeCl₃·6H₂O and RhCl₃·3H₂O. To prepare the precursor, the reactants were mixed with NaCl, which is ten times the mass of the reactants and works as the disperse medium, dissolved in deionized water and then dried at 60 °C for 48 hours to be desiccated. After being ground, the precursor was sintered at 750 °C for 3 hours in hydrogen furnace, which was followed by washing, centrifugation and arefaction. Finally, the product was heated to 750 °C with a heating rate of 10 °C/min and duration of 48 hours in vacuum to exclude hydrogen atoms dissolved in the sample. The powdery Fe-Rh of other elemental compositions were

synthesized in the same way as mentioned above by changing the mole ratio of FeCl₃·6H₂O and RhCl₃·3H₂O correspondingly.

The structure of the particles was characterized by powder X-ray diffraction (XRD) using a DX-2700 diffractometer with Cu K_{α} radiation. The XRD patterns were collected in the 2θ range of 25 - 90 ° with a step size of 0.02 °. The Rietveld diffraction profile fitting technique was employed to refine the crystal structure by means of the Rietica software. The magnetic properties were measured by a vibrating sample magnetometer (VSM) with a maximum applied field of 3 T and the temperature ranging from 70 to 370 K and room temperature to 750 K. Scanning electron microscope (SEM) and energy dispersive X-ray spectroscopy (EDX) measurements were used to observe the microstructure and composition of the samples, respectively. The preliminary *in vitro* biological toxicity of FeRh particles was investigated with standard MTT assay.

Results and Discussion

Fig.1 shows the X-ray diffraction patterns of the five binary Fe_xRh_{100-x} particulate alloy samples with compositions for x = 50, 48, 45, 40, and 35, respectively, after reducing and annealing at 750 °C in dynamic vacuum. The two sets of vertical bars at the bottom are the calculated Bragg diffraction peaks of the chemically-ordered FeRh α' phase with CsCl-type structure (PDF 03-065-0986) and the Rh-rich Fe₃Rh₇ solid solution γ phase with face-centered cubic (fcc) structure (PDF 03-065-7228). The indices of the crystalline planes for the two component phases are labeled on the top of the figure. The superlattice diffraction peaks at $2\theta = 29.8^{\circ}$ and 53.1° verify that the

particulate equiatomic Fe $_{50}$ Rh $_{50}$ adopts ordered CsC1-type α' phase. ¹⁶ The sample can be considered as single-phase structure within the resolution of the XRD since no additional diffractions can be observed except for the α' phase. However, with higher Rh content, a diffraction peak located at $2\theta = 41.5^{\circ}$ presents and indicates the presence of the fcc γ phase.

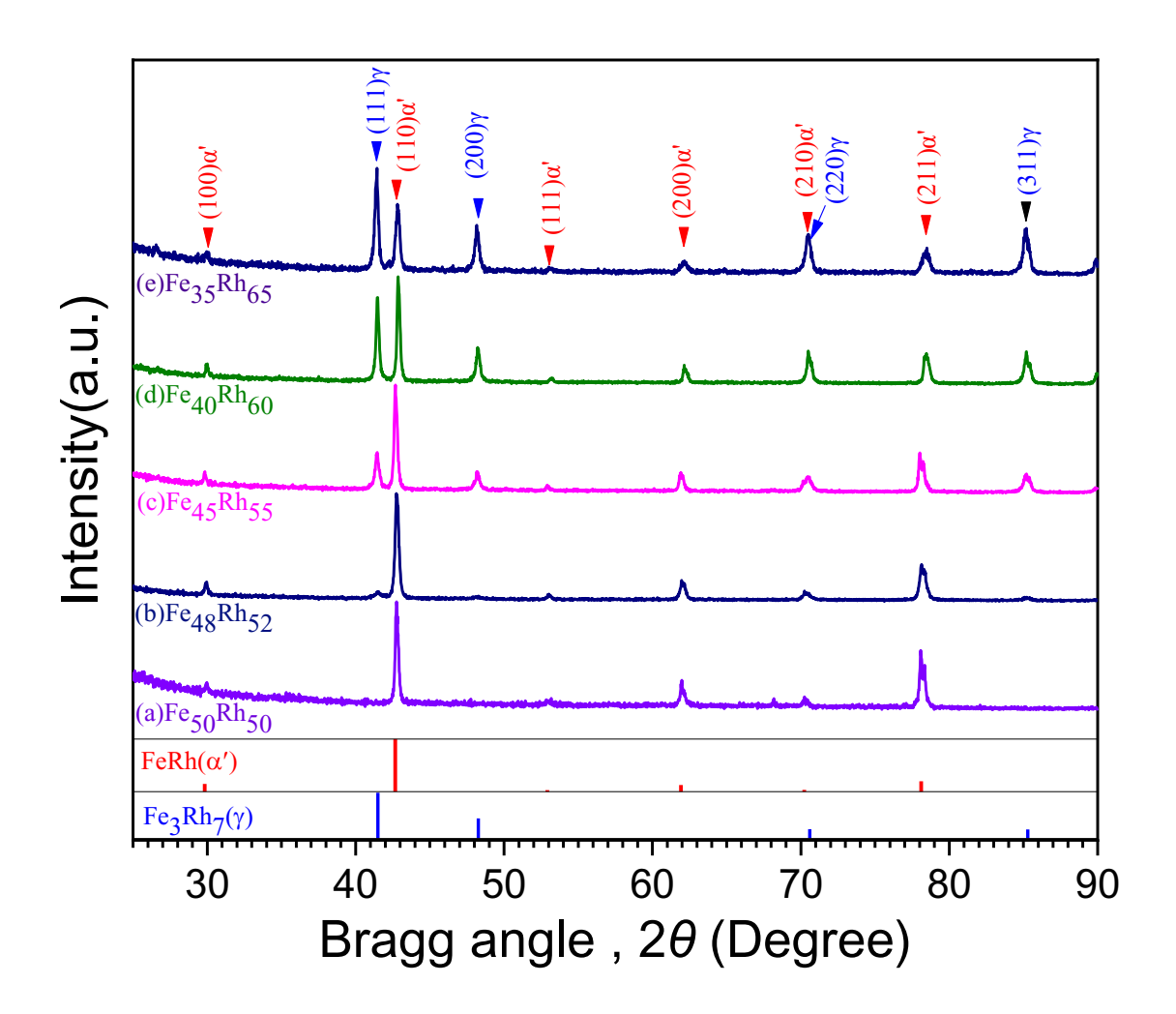


Fig.1. X-ray diffraction patterns of the particulate samples (a) Fe₅₀Rh₅₀; (b) Fe₄₈Rh₅₂; (c) Fe₄₅Rh₅₅; (d) Fe₄₀Rh₆₀; (e)Fe₃₅Rh₆₅ annealed at 750 °C in vacuum. The calculated diffraction peaks of FeRh and Fe₃Rh₇ phases are displayed at the bottom.

After Rietveld refinement the cell parameters and the phase compositions of the

studied samples are listed in Table 1. For the Fe₅₀Rh₅₀ alloy, the cell parameter is of a = 2.9962 Å, which is comparable to that of 2.9930 Å in literature. 17 With the growth of the Rh content, the cell constant of the α' phase increases slightly and reaches maximum 3.0066 Å when x = 45. Then, it decreases with the further rise of Rh. The variation of the cell constant of the α' phase can be caused by two reasons. One is the chemical substitution. Transition metals, such as Pd, Ni, and Pt, can modify the cell parameter through substitution for Fe or Rh. 15 The other one is the magnetic state. The cell expands about 0.3% during the phase transition from AFM to FM for the α' phase. Therefore, in Table 1, the greater constants of the α' phase for x = 50, 48, and 45 can be ascribed to the increase of Rh whose atomic radius, 1.34 Å, is greater than that of iron, 1.26 Å. The smaller values for x = 40, and 35 can be mainly understood by their AFM state at room temperature, which will be illustrated in Fig. 2 and discussed in detail afterward. Furthermore, as the Rh content rises, the cell constants of the γ phase go up and the values are between those of Fe₃Rh₇ (a = 3.7717 Å) and pure Rh (a = 3.8031 Å). The γ phase component also increases as illustrated by the intensity of the γ diffraction peaks.

Table 1. Cell parameters and phase percentage of the Fe_xRh_{100-x} (x = 50, 48, 45, 40, 35) alloys.

	Cell parameter		Molar percentage	
Sample	(Å)		(%)	
	α'	γ	α'	γ
Fe ₅₀ Rh ₅₀	2.9962		100	0
$Fe_{48}Rh_{52}$	3.0036	3.7745	97.03	2.97
$Fe_{45}Rh_{55}$	3.0066	3.7779	79.41	20.59
$Fe_{40}Rh_{60}$	2.9846	3.7887	71.19	28.81
$Fe_{35}Rh_{65}$	2.9874	3.7889	61.71	38.29

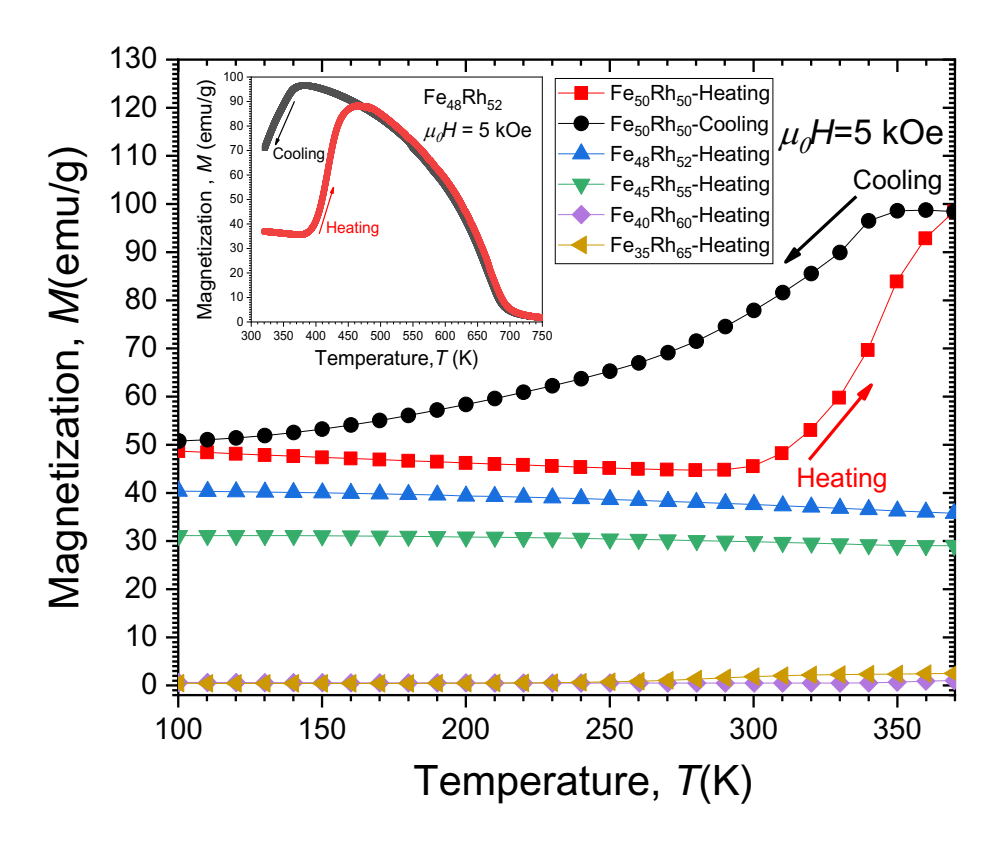


Fig.2. Temperature dependences of magnetization of Fe_xRh_{100-x} (x = 50, 48, 45, 40, 35) particulate alloys under a 5 kOe applied field.

The temperature dependent magnetization curves under a 5 kOe external field for the five Fe-Rh alloys in the temperature range of $100 \sim 370$ K are plotted in Fig.2. It was seen that only the Fe₅₀Rh₅₀ sample displays first-order AFM-FM phase transition in the measured temperature range. In the heating process, the magnetization starts to increase when the temperature exceeds 300 K and it keeps rising till the highest temperature 370 K. During cooling, the magnetization declines slowly and returns to the initial value of heating as the sample is cooled down to 100 K. Large hysteresis and evident asymmetry are clearly observed. However, the transition during heating is incomplete due to the temperature limitation of the set-up. To know more details of the first-order transition for the Fe₄₈Rh₅₂ sample, measurements on thermal magnetization in the higher temperature range from room temperature to 750 K was

performed and the results are shown in the insert. For the AFM-FM transition of Fe₄₈Rh₅₂, the magnetization goes up near 380 K from 35.6 emu/g to maximum 88.8 emu/g near 464 K. Therefore, the AFM-FM transition span is about 80 K which is much wider than that of the bulk samples. After that, the magnetization decreases and when temperature is raised to 750 K the magnetization goes down to zero approximately, signifying the sample is PM above that temperature. The zero magnetization above 750 K indicates that there is no ferromagnetic Fe-based disordered solid solution bcc α phase with the Curie temperature above 1000 K in the sample.¹⁹ It is consistent with the x-ray analysis in Fig. 1. In the cooling process, the magnetization goes down below 375 K and the hysteresis is about 89 K (= 464–375 K). In contrast, for bulk binary Fe-Rh alloys, the first-order transition is abrupt and the hysteresis is only about 10 K.²⁰ So, the particulate samples exhibit broader transition and greater hysteresis compared with the bulk counterparts. Considering the ordered α' phase detected by XRD in Fig. 1, the samples of x = 48, 45, 40, and 35 are expected to have first-order AFM-FM transitions in temperatures above 370 K. High transition temperature is not beneficial for potential application near room or human body temperature and the magnetocaloric effect for x = 48, 45, 40, and 35 are not characterized furtherly.

Additionally, in Fig. 2, when the temperature is ~ 100 K significant values of magnetization, 48, 40, and 31 emu/g, are still observed for the samples with x = 50, 48, and 45, respectively. For Fe₃₅Rh₆₅ and Fe₄₀Rh₆₀, the magnetizations are almost zero and no phase transition takes place within the investigated temperature range. This

suggests the stabilization of FM occurs for the three Fe-rich samples. ^{21,22} The residual magnetization is absent in bulk Fe-Rh alloys but it was previously reported in the Fe-Rh films and found out to be thickness dependent. 23,24 When the film thickness is under 10 nm, large amount of magnetization presents below the FM-AFM transition temperature. y phase is PM at all measured temperatures, therefore, the residual magnetization must come from the ordered α' phase. This can be interpreted by the following reasons. Liu and coworkers showed the important role played by the surface configuration in the morphology of FeRh nanoparticles (NPs) and in the stabilization of the FM state, which is accounted for the enhanced polarization of Rh at the large Rh-terminated (100) surface facets.²⁵ In addition, from the Fe-Rh binary diagram, two types of chemically ordered α' phases with ferromagnetism and antiferromagnetism, respectively, could present in the near-equiatomic alloys due to the insufficient diffusion and thus cause small difference in composition. Their cell parameters are too close for them to be distinguished by x-ray diffraction.²⁶ In our results, the broad AFM-FM transition in Fig. 1 inset for the Fe₄₈Rh₅₂ sample reflects their coexistence.

To clarify the reason for the residual FM after the FM-AFM transition, the SEM microstructure and EDS measurements were performed on Fe₅₀Rh₅₀ sample annealed at 750 °C in vacuum. In Fig. 3, it is seen that after annealing the particles are about 100 to 200 nm in dimensions and they aggregate to form micron clusters about 800-1000 nm. EDS analysis on the cluster surface shows that the atomic ratio of iron to rhodium is about 65:35. Noteworthily, our XPS measurements (not shown) also

suggested the higher iron content on the sample surface. In the binary diagram, Fe-Rh alloys with Fe content near 65 at. % are also chemically ordered but ferromagnetic, which explains the considerable magnetization of the samples at low temperatures. However, AFM-FM transition is indeed observed (see Fig. 2), which illustrates that the concentration of some particles is closely equiatomic. Therefore, the greater iron content at the surface suggests the concentrations of the two elements is nonuniform within the particles and clusters. In addition, we note that the residual magnetization in Fig.2 is composition dependent. With increasing Rh content, the residual magnetization drops and then approaches zero when it is more than 60 at. % Rh. On the one hand, more Rh atoms can balance the surface concentration to obtain more phase with AFM magnetic structure. On the other hand, the presence of secondary γ phase are beneficial to modify the surface structure of the main phase and reduce the ferromagnetic moments of iron near the surface.



Fig.3. SEM microstructure of the Fe₅₀Rh₅₀ sample.

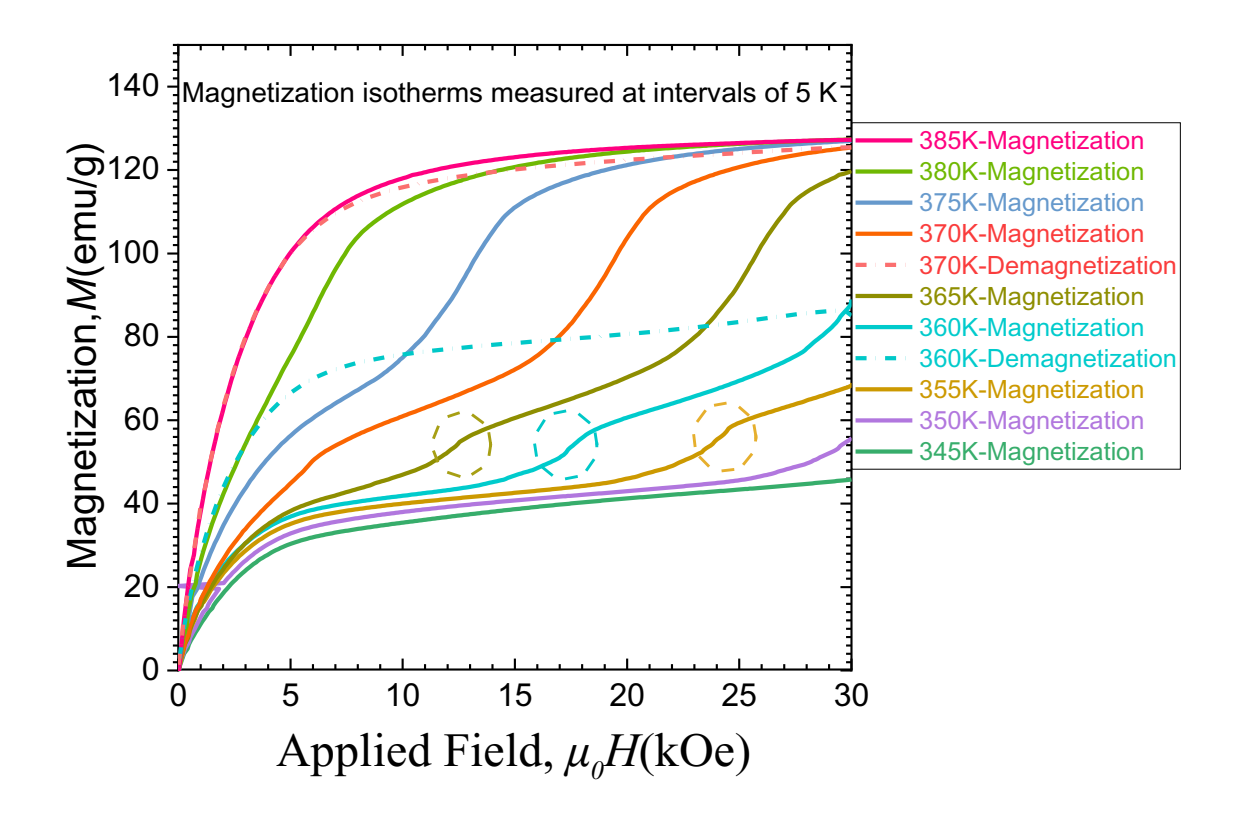


Fig.4. Isothermal magnetization curves of the Fe₅₀Rh₅₀ particulate sample in the temperature range of 345-385 K under an applied magnetic field 0 to 3 T.

Fig.4 presents the magnetization of FeRh particles as a function of external field at discrete temperatures in the range of 345-385 K, in the vicinity of the transition temperature. For clarity, only the demagnetization curves at 360 and 370 K are displayed. From Fig.2, it is known that below 345 K the Fe₅₀Rh₅₀ alloy is predominantly antiferromagnetic with secondary ferromagnetism. In Fig. 4, the magnetization at 345 K shows the ferromagnetic feature, *i.e.* magnetization increasing rapidly with applied field and then approaching saturation. The magnetization rises to about 40 emu/g as the magnetic field increases to 3 T at 345 K. With the temperature increasing from 350 to 375 K, the field-driven metamagnetic transition from AFM to FM with step-like magnetization can be clearly observed. It is worth mentioning that

in Fig. 4 small steps, indicated by the dash circles, can be observed near 24, 17, and 12 kOe on the magnetization isotherms at 355, 360, and 365 K, respectively. They have never been reported in the film or bulk Fe-Rh materials. As suggested by the EDS measurements, the inhomogeneous distribution of elements takes the responsibility.

In Fig. 4, for the demagnetization curves at 360 and 370 K, no step-like reverse transitions can be observed. One can assume that the FM part resulted from the AFM-FM transition may not go back to the AFM state after the removal of magnetic field. According to our measurements (not shown), if the next magnetization isotherm is followed by the previous demagnetization, most of magnetization nearly overlaps with the previous demagnetization and thus makes the formed area between two magnetization isotherms unusual large and results in abnormally large magnetic entropy change. In this study, in order to avoid overestimating the entropy change, the optimized method of measurement is adopted. Namely, for each isothermal magnetization, the sample was cooled down to the lowest temperature which is 70 K without any applied field and then heated up to the next expected temperature and the magnetization and demagnetization curves were measured as a function of an applied field.

The negative magnetocaloric effect in terms of isothermal magnetic entropy changes (ΔS_{mag}) with different applied fields are shown in Fig.5. They were calculated from the isothermal magnetization curves by employing Maxwell's relation.²⁷ The occurring temperatures of ΔS_{mag} maximum almost decrease with the increasing of the

applied filed, which substantially reflects the first-order AFM-FM transition. When the applied field is 3.0, 2.0, and 1.0 T, the $\Delta S_{\rm mag}$ peak reaches about 9.7, 7.8, and 4.0 J/kgK, respectively. For the bulk Fe₅₀Rh₅₀ alloy, it is 16.37 J/kgK occurring at about 392 K at 2 T.³ Therefore, $\Delta S_{\rm mag}$ of our particulate sample is half of the bulk counterpart. This is understandable due to the noticeable residual FM phase below the FM-AFM transition temperature (see Fig.2), which has no contribution to the magnetocaloric effect near the transition. The relative cooling powers (*RCPs*) are 211, 125, and 62 J/kgK at fields of 3, 2, and 1 T, respectively. Despite of its lower $\Delta S_{\rm mag}$ values compared to the bulk samples, particulate Fe₅₀Rh₅₀ prevails over other magnetocaloric materials whose transition temperature is over human body temperature 310 K in the low-field $\Delta S_{\rm mag}$ and *RCP*.²⁸

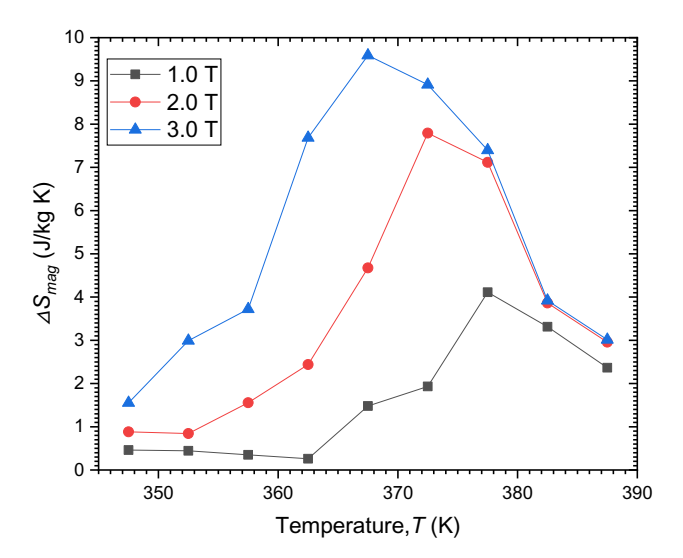


Fig.5. Temperature dependence of the magnetic entropy change (ΔS_{mag}) of the Fe $_{50}$ Rh $_{50}$ particles with the magnetic field change of 0-3 T.

The cytotoxicity of FeRh samples were tested by MTT assay and the results are shown in Fig. 6. FeRh particles synthesized by solid phase reduction possessed higher

cell viability compared with the arc-melted bulk samples. Cell viability higher than 80% can be seen in the particles. It demonstrated that solid phase reduction is an ideal method to fabricate FeRh materials that possess low cytotoxicity and meet requirements for biomedical uses.

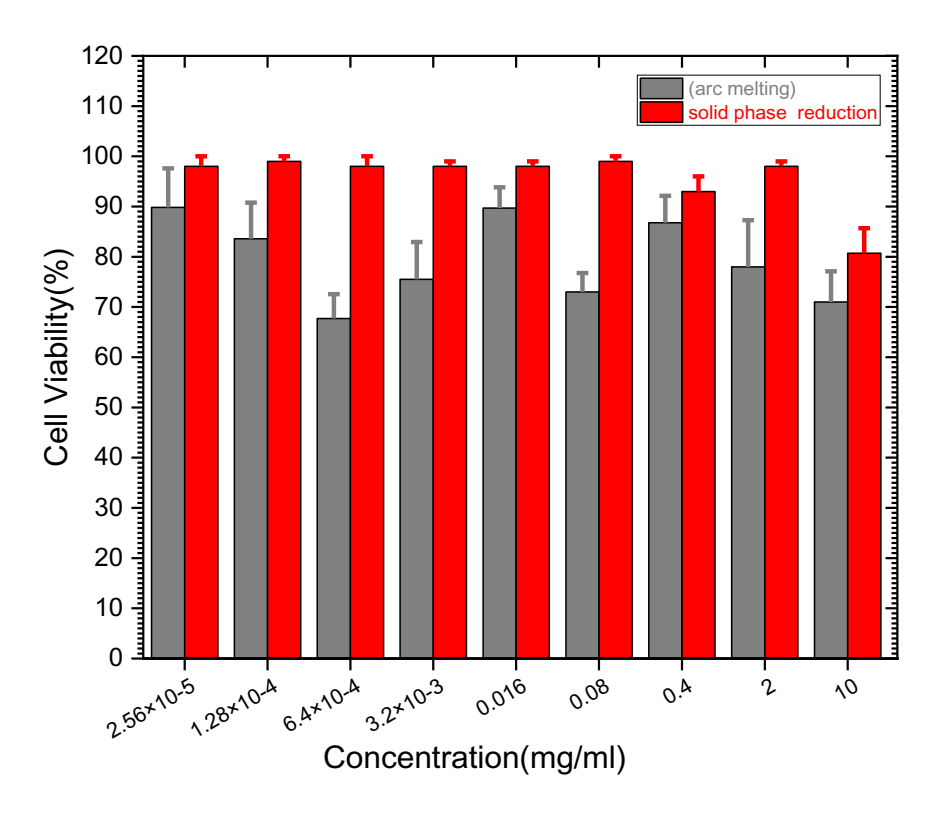


Fig.6. Cell Viability for the arc melting and solid phase reduction produced FeRh samples at different concentrations in MTT assay test.

3. Conclusions

A series of particulate Fe_xRh_{100-x} alloys (x = 50, 48, 45, 40, 35) were synthesized by high temperature solid state reaction and their structure and magnetic properties and magnetocaloric effect characterized. Only $Fe_{50}Rh_{50}$ particles possess single α' phase structure and the rest Fe_xRh_{100-x} samples have secondary γ phase whose content is proportional to Rh content. First-order transition with large thermal hysteresis was

observed in Fe $_{50}$ Rh $_{50}$ and Fe $_{48}$ Rh $_{52}$ particles. The elements distribute inhomogeneously in the samples and there is more Fe on the surface, which could be an explanation for the unusual residual magnetization below the transition temperature and the extra steps in the isothermal magnetization curves. The further analysis on Fe $_{50}$ Rh $_{50}$ particles reveals a ΔS_{mag} maximum of about 9.7 J/Kg·K and an *RCP* of almost 230 J/kg under a magnetic field change of 0 to 3 T. The result of MSST test supports the possible feasibility of Fe-Rh particles use for living tissues and cells.

Acknowledgments

This work was supported by the National Natural Science Foundation of China (Nos. 51901036 and 51750110501) and the Fundamental Research Funds for the Central Universities (No. ZYGX2019J099).

Reference

¹ S. A. Nikitin, G. Myalikgulyev, A. M. Tishin, M. P. Annaorazov, K. A. Asatryan, and A. L. Tyurin, Phys. Lett. A. **148** (6), 363 (1990).

² P. A. Algarabel, M. R. Ibarra, C. Marquina, A. del Moral, J. Galibert, M. Iqbal, and S. Askenazy, Appl. Phys. Lett. **66** (22), 3061 (1995).

³ Radhika Barua, Félix Jiménez-Villacorta, and L. H. Lewis, J. Appl. Phys. **115** (17), 17A903 (2014).

⁴ Radhika Barua, Xiujuan Jiang, Felix Jimenez-Villacorta, J. E. Shield, D. Heiman, and L. H. Lewis, J. Appl. Phys. **113** (2), 023910 (2013).

⁵ H. Y. Y. Ko and T. Suzuki, J. Appl. Phys. **101** (9) (2007).

⁶ H. Y. Y. Ko, T. Suzuki, N. T. Nam, N. N. Phuoc, J. Cao, and Y. Hirotsu, J. Magn. Magn. Mater. **320** (22), 3120 (2008).

⁷ H. Y. Y. Ko, T. Suzuki, N. N. Phuoc, and J. W. Cao, J. Appl. Phys. **103** (7) (2008).

⁸ Z Jia, JW Harrell, and RDK Misra, Appl. Phys. Lett. **93** (2), 022504 (2008).

- ⁹ Radhika Barua, Felix Jimenez-Villacorta, J. E. Shield, D. Heiman, and L. H. Lewis, J. Appl. Phys. 113 (17), 17B523 (2013).
- ¹⁰ C. F. Sánchez-Valdés, R. R. Gimaev, M. López-Cruz, J. L. Sánchez Llamazares, V. I. Zverev, A. M. Tishin, A. M. G. Carvalho, D. J. M. Aguiar, Y. Mudryk, and V. K. Pecharsky, J. Magn. Magn. Mater., 166130 (2019).
- ¹¹ A. M. Tishin, Y. I. Spichkin, V. I. Zverev, and P. W. Egolf, Int. J. Refrig. **68**, 177 (2016).
- ¹² A. M. Tishin, patent EP 1897590 B1 (2016).
- ¹³ A. M.Tishin, Yu. A.Rochev, and A. V. Gorelov, Patent US9, 017713 B2 (2015).
- ¹⁴ V. I. Zverev, A. P. Pyatakov, A. A. Shtil, and A. M. Tishin, J. Magn. Magn. Mater. **459**, 182 (2018).
- ¹⁵ Y. Ohtani and I. Hatakeyama, J. Magn. Magn. Mater. **131** (3), 339 (1994).
- ¹⁶ I. Suzuki, T. Koike, M. Itoh, T. Taniyama, and T. Sato, J. Appl. Phys. **105** (7) (2009).
- ¹⁷ S. Maat, J. U. Thiele, and E. E. Fullerton, Phys. Rev. B **72** (21) (2005).
- ¹⁸ S. A. Makhlouf, T. Nakamura, and M. Shiga, J. Magn. Magn. Mater. **135** (3), 257 (1994).
- ¹⁹ A.I. Zakharov, A.M. Kadomtseva, R.Z. Levitin, and E.G. Ponyatovskii, Sov. Phys. JETP 19, 1348 (1964).
- ²⁰ H. Okamoto, J. Phase Equilib. Diff. **32** (5), 472 (2011).
- ²¹ R. Barua, F. Jimenez-Villacorta, and L. H. Lewis, Appl. Phys. Lett. 103 (10) (2013).
- Jiangwei Cao, Nguyen T. Nam, Sho Inoue, Hnin Yu Yu Ko, Nguyen N. Phuoc, and Takao Suzuki, J. Appl. Phys. 103 (7), 07F501 (2008).
- ²³ A. Chirkova, F. Bittner, K. Nenkov, N. V. Baranov, L. Schultz, K. Nielsch, and T. G. Woodcock, Acta Mater. **131**, 31 (2017).
- ²⁴ I. Suzuki, T. Koike, M. Itoh, T. Taniyama, and T. Sato, J. Appl. Phys. **105** (7) (2009).
- M. Liu, P. Benzo, H. Tang, M. Castiella, B. Warot-Fonrose, N. Tarrat, C. Gatel, M. Respaud, J. Morillo, and M. J. Casanove, EPL. 116 (2) (2016).
- ²⁶ V. I. Zverev, A. M. Saletsky, R. R. Gimaev, A. M. Tishin, T. Miyanaga, and J. B. Staunton, Appl. Phys. Lett. **108** (19), 192405 (2016).
- ²⁷ V. K. Pecharsky and K. A. Gschneidner, J. Appl. Phys. **86** (1), 565 (1999).
- ²⁸ S. Y. Dan'kov, A. M. Tishin, V. K. Pecharsky, and K. A. Gschneidner, Phys. Rev. B 57 (6), 3478 (1998).

Highlights

- FeRh particles were successfully synthesized by solid state reaction.
- First-order transition was observed in Fe₅₀Rh₅₀ and Fe₄₈Rh₅₂ particles.
- \triangleright - $\Delta S_{\rm M}$ of 9.7 J/kg K and RCP of 230 J/kg (0-3T) was obtained for Fe₅₀Rh₅₀ particles.
- MSST test supports the possible feasibility of Fe-Rh particles for biomedical use.

*Declaration of Interest Statement

De	eclaration of interests			
\Box The authors declare that they have no known competing financial interests or personal relationships that could have appeared to influence the work reported in this paper.				
	The authors declare the following financial interests/personal relationships which may be considered potential competing interests:			
	All authors, Yutao Cao, Yue Yuan, Yafen Shang, Vladimir I. Zverev, Radel R. Gimaev, R.			
	Barua, R. L. Hadimani, Lan Mei, Gang Guo, Hao Fu declare no conflict of interest.			

Hao Fu: Conceptualization, Resources, Writing - Review & Editing, Funding acquisition, Project administration, Supervision

Yutao Cao: Methodology, Investigation, Data Curation, Writing - Original Draft, Visualization

Yue Yuan: Investigation, Writing - Original Draft, Visualization

Yafen Shang: Writing - Review & Editing

Vladimir I. Zverev: Writing - Review & Editing

Radel R. Gimaev: Writing - Review & Editing

R. Barua: Writing - Review & Editing

R. L. Hadimani: Writing - Review & Editing

Lan Mei: Writing - Review & Editing, Resources

Gang Guo: Writing - Review & Editing Resources